Multilayer-coated diffraction gratings: differential method of Chandezon *et al.* revisited

Lifeng Li

Optical Sciences Center, University of Arizona, Tucson, Arizona 85721

Received February 28, 1994; revised manuscript received May 2, 1994; accepted May 16, 1994

I report significant improvements to the differential method of Chandezon *et al.* [J. Opt. Soc. Am. **72**, 839–846 (1982)]. The R-matrix propagation algorithm is used to remove completely the previously existing limitations on the total coating thickness and on the total number of coated layers. I analyze the symmetry properties of the eigenvalue problem that arises in the differential formalism and use them to speed up the numerical computation. The time needed for computing the eigensolutions of coated gratings in a conical mount is reduced to little more than what is needed for gratings in a classical mount. For gratings with dielectric coatings or gratings with symmetrical profiles the need to invert certain matrices appearing in the formalism is eliminated. Numerical results show that it is possible to make nearly 100% efficient surface-relief reflection gratings in a Littrow mount by the use of dielectric materials only.

1. INTRODUCTION

In many applications, practitioners coat surface-relief gratings with one or more dielectric layers to enhance diffraction efficiency and, in the case of metallic gratings, to prevent the metallic grating surface from tarnishing. If the thicknesses of the individual coated layers are small fractions of the grating period, the contours of the medium interfaces tend to follow that of the periodically corrugated initial grating surface. In this paper gratings that consist of multiple periodically corrugated medium interfaces are referred to as coated gratings.

Coated gratings, compared with bare (single-periodic-interface) gratings, present certain analytical difficulties that not every grating method is equipped to deal with. For example, the classical modal method[1] and the coupled-wave method,[2] which rely on approximating a smooth grating profile by a succession of lamellar gratings, are inherently inefficient in dealing with coated gratings. Only those methods, such as the integral method[3,4] and the extinction-theorem method,[5] that explicitly take the grating contour into account are naturally suited for coated gratings. However, the integral method is limited to gratings whose number of coated layers is not much greater than 3,[6] and the extinction-theorem method is limited to gratings of shallow groove depth.[7] In the early 1980's Chandezon *et al.*[6,8] presented a new differential formalism for multicoated gratings that was applicable in the entire optical region. Subsequently, the method was generalized to conical mountings by Popov and Mashev[9] and at a later time by Elston *et al.*[10] Popov and Mashev also numerically investigated the convergence of the method[11,12] and experimentally investigated the diffraction efficiency anomalies of multilayer-coated dielectric gratings.[13] In this paper, following Refs. 11 and 12, the method of Chandezon *et al.* is referred to as the C method.

Chandezon *et al.* acknowledged in their paper[6] that numerical problems prevented them "from achieving the computations when the total thickness of dielectric exceeds one wavelength, or when the number of layers exceeds eight." They further stated that "these limitations could be modified by using more-sophisticated numerical techniques." In the present paper I have completely removed these limitations by incorporating a numerical technique that is called the R-matrix propagation algorithm[1,5] into the C method. In addition, by analyzing the symmetry properties of the eigenvalue problem appearing in the C method, I have reformulated part of the mathematical development of the C method so that the computation time is significantly reduced, especially for gratings in conical mountings.

2. NOTATION

A multilayer-coated grating in a conical diffraction mount, along with the Cartesian and polar coordinate systems, is illustrated in Fig. 1. The notation for the media and their interfaces is shown in Fig. 2, where $Q \geq 0$ is the total number of coatings. For the sake of generality, it is assumed that there are $L \geq 0$ planar layers above the top corrugated surface and $-P \geq 0$ planar layers below the bottom corrugated surface. In this paper, whenever possible, subscripts are reserved for the physical and mathematical quantities in the corrugated region, and superscripts with parentheses are reserved for the quantities above and below the corrugated region. In the upper curved-to-planar transition layer the subscript $Q+1$ and the superscript $(+1)$ are used interchangeably, and a similar convention holds for the subscript 0 and the superscript (-1) in the lower transition layer. The location of a curved interface is specified by the ordinate of its minimum, y_j. The thicknesses of the layers are denoted by

$$e_j = \begin{cases} y_0 - y^{(-1)} & j = 0 \\ y_j - y_{j-1} & 1 \leq j \leq Q \\ y^{(+1)} - y_Q & j = Q+1 \end{cases}, \tag{1a}$$

$$e^{(j)} = \begin{cases} y^{(j)} - y^{(j-1)} & +2 \leq j \leq L \\ y^{(j+1)} - y^{(j)} & P \leq j \leq -2 \end{cases}. \tag{1b}$$

0740-3232/94/112816-13$06.00

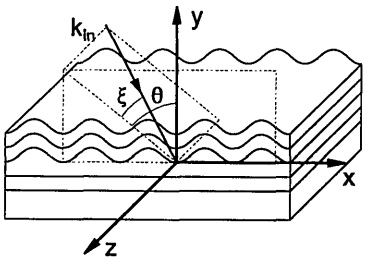

Fig. 1. Multilayer-coated grating in a conical mount.

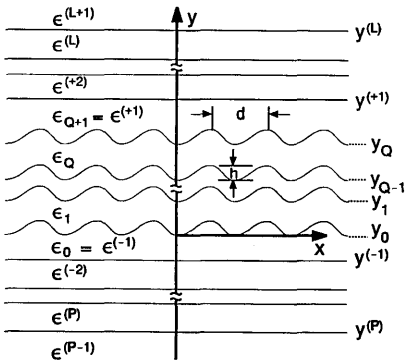

Fig. 2. Notation for the media and medium interfaces of a multilayer-coated grating.

Although the magnetic permeabilities for most optical materials are unity (the Gaussian system of units is used in this paper), I permit them here to be different from unity and from each other to maximize the generality of the theory and to preserve certain symmetries between the electric and magnetic fields in the mathematical formulas to be derived. The incident light is assumed to be a monochromatic, arbitrarily polarized plane wave having a time-dependent factor $\exp(-i\omega t)$.

The grating profile function $a(x) \geq 0$ can be an arbitrary periodic function of x as long as the Fourier expansions of functions $C(x)$ and $D(x)$, to be defined at the end of this section, converge. All corrugated interfaces are assumed to have the same functional form except for their vertical offsets. Thus the contour of the jth curved interface is given by

$$y = y_j + a(x), \qquad 0 \leq j \leq Q. \tag{2}$$

The grating groove depth and the period are denoted by h and d, respectively.

Next I define various wave vectors. The modulus squared of the wave vectors in all media is conventionally given by

$$k_j^2 = \epsilon_j \mu_j \kappa^2, \qquad 0 \leq j \leq Q+1, \tag{3a}$$

$$k^{(j)2} = \epsilon^{(j)} \mu^{(j)} \kappa^2, \qquad +1 \leq j \leq L+1 \text{ or } P-1 \leq j \leq -1, \tag{3b}$$

where $\kappa = 2\pi/\lambda$, λ being the vacuum wavelength. For simplicity, hereafter only the formula with subscripts or superscripts will be given whenever the formula is valid in both the curved and planar regions, and, unless specified otherwise, the index j runs in the ranges given in Eq. (3a) or (3b) depending on the spatial regions under consideration. For a given grating a conical mount is uniquely defined by the wave vector of the incident plane wave

$$\mathbf{k}_{\text{in}} = \hat{x}\alpha_0 - \hat{y}\beta_0^{(L+1)} + \hat{z}k_z, \tag{4}$$

where, from Fig. 1, $\alpha_0 = k^{(L+1)} \sin\theta \cos\xi$, $\beta_0^{(L+1)} = k^{(L+1)} \cos\theta \cos\xi$, and $k_z = k^{(L+1)} \sin\xi$. Since the grating structure is invariant in the z direction, the z-dependent factor $\exp(ik_z z)$ is shared by the fields everywhere.

For an incident wave vector with $k_z \neq 0$ a reduced incident wave vector and the modulus squared of the reduced wave vectors in all media can be defined as

$$\mathbf{k}_{\text{in}}' = \hat{x}\alpha_0 - \hat{y}\beta_0^{(L+1)}, \tag{5}$$

$$\tilde{k}_j^2 = k_j^2 - k_z^2, \tag{6}$$

respectively. In this paper, for a given conical mount, a classical mount is called the induced mount (by the conical mount) if its incident wave vector has identical x and y components to those of the conical mount. It will be shown in Section 4 that the mathematical analysis of a grating in a conical mount is intimately related to the analysis of the same grating in the induced classical mount.

The content of this paper is quite mathematical. For the sake of clarity, I list some of the notation below. Additional notation will be introduced as needed.

N: Truncation order, i.e., the number of the Rayleigh orders that are retained in the numerical computation.
Superscript T: Matrix transpose.
Superscript $*$: Matrix adjoint.
Superscript s: $s = e$ and $s = h$ denote the z components of the electric- and magnetic-field vectors, respectively, of the incident and diffracted Rayleigh amplitudes. They are also used to denote, respectively, the $H_\perp$-type and $E_\perp$-type eigenvalues and eigenvectors of the quasi-Rayleigh waves (this term is defined in Subsection 3.B).
$R_n^{(s)}$ and $T_n^{(s)}$: Rayleigh amplitudes for the diffracted orders in the uppermost and lowermost media, respectively.
$I_n^{(s)}$ and $J_n^{(s)}$: Rayleigh amplitudes for the incident orders in the uppermost and lowermost media, respectively. In most applications $J_n^{(s)} = 0$ for all n, and $I_n^{(s)} \neq 0$ only if $n = 0$. However, in order to preserve the symmetry of many formulas to be derived with respect to $I_n^{(s)}$ and $J_n^{(s)}$, I postpone the above substitutions until the numerical implementation.
U and V: Sets of integers designating the Rayleigh and quasi-Rayleigh orders after truncation, respectively.
$U^{(\pm 1)}$: Set of integers designating the propagating Rayleigh orders in medium (± 1).
$V^{(\pm 1)}$: Set of integers designating the upward and downward decaying quasi-Rayleigh orders in medium (± 1) after truncation, respectively.

$$\tau_1^{(j)} = i\frac{\kappa^2 \epsilon^{(j)}}{\tilde{k}^{(j)2}}, \qquad \tau_2^{(j)} = i\frac{\kappa^2 \mu^{(j)}}{\tilde{k}^{(j)2}}, \qquad \tau_3^{(j)} = i\frac{\kappa k_z}{\tilde{k}^{(j)2}};$$

$$K = 2\pi/d;$$

$\alpha_m = \alpha_0 + mK$, where m is an integer;

$$\beta_m^{(j)} = [\tilde{k}^{(j)2} - \alpha_m^2]^{1/2}, \qquad \text{Re}[\beta_m^{(j)}] + \text{Im}[\beta_m^{(j)}] \geq 0;$$

$$C(x) = \frac{1}{1 + \dot{a}^2(x)} = \sum_{m=-\infty}^{\infty} C_m \exp(imKx),$$

$$C_m = \frac{1}{d} \int C(x)\exp(-imKx)\mathrm{d}x; \tag{7}$$

$$D(x) = \frac{\dot{a}(x)}{1 + \dot{a}^2(x)} = \sum_{m=-\infty}^{\infty} D_m \exp(imKx),$$

$$D_m = \frac{1}{d} \int D(x)\exp(-imKx)\mathrm{d}x. \tag{8}$$

The integrations in Eqs. (7) and (8) are over one grating period.

3. DIFFERENTIAL METHOD OF CHANDEZON *ET AL.*

The purpose of this section is to review the differential method of Chandezon *et al.* and thereby to lay down the appropriate framework for its further development in Section 4. In Subsections 3.A and 3.B all layer-identifying subscripts are omitted. In addition, throughout this paper I use representative vector and matrix elements with subscripts to denote the respective vectors and matrices.

A. Field in a Planar Layer

In a planar layer it is legitimate to write the z components of the fields in Rayleigh expansions. Because of the invariance of the grating geometry with respect to z, the x components of the fields can then be expressed in terms of the z components. In this paper the column vector defined by

$$F(y) = \left(E_{zm}, H_{zm}, \frac{\kappa}{i} H_{xm}, \frac{\kappa}{i} E_{xm}\right)^T \tag{9}$$

is called an F vector, where $m \in U$. It can be shown that

$$F(y) = W\phi(y - y')W^{-1}F(y'), \tag{10}$$

where y' is a constant, ϕ is a diagonal matrix,

$$\phi(y) = \exp(+i\beta_m y) \oplus \exp(+i\beta_m y) \oplus \exp(-i\beta_m y) \oplus \exp(-i\beta_m y), \tag{11}$$

$$W = \begin{bmatrix} 1 & 0 & 1 & 0 \\ 0 & 1 & 0 & 1 \\ -\tau_1\beta_m & \tau_3\alpha_m & \tau_1\beta_m & \tau_3\alpha_m \\ \tau_3\alpha_m & \tau_2\beta_m & \tau_3\alpha_m & -\tau_2\beta_m \end{bmatrix}, \tag{12}$$

with 1 representing the identity matrix, 0 representing the zero matrix, and all other entries being diagonal matrices. In Eq. (11) the symbol $\oplus$ means matrix direct sum.

B. Field in a Curved Layer

The ingenuity of the C method is to solve Maxwell's equations for the fields in regions bound by curved surfaces in a curvilinear coordinate system $Oxuz$, where x and z are unchanged from the Cartesian coordinates in Fig. 1 but y is replaced by

$$u = y - a(x). \tag{13}$$

In this curvilinear system the grating interfaces coincide with the coordinate surfaces $u = y_j$. By the use of Maxwell's equations in the tensorial covariant form[14] the following equations can be derived[9,10]:

$$\frac{\partial E_z}{\partial u} = D(x)\frac{\partial E_z}{\partial x} + \frac{i}{\kappa\epsilon} C(x)\left(\tilde{k}^2 H_x - ik_z \frac{\partial H_z}{\partial x}\right), \tag{14a}$$

$$\frac{\partial H_z}{\partial u} = D(x)\frac{\partial H_z}{\partial x} - \frac{i}{\kappa\mu} C(x)\left(\tilde{k}^2 E_x - ik_z \frac{\partial E_z}{\partial x}\right), \tag{14b}$$

$$\frac{\partial H_x}{\partial u} = \frac{\partial}{\partial x}[D(x)H_x] + i\kappa\epsilon E_z - \frac{i}{\kappa\mu}\frac{\partial}{\partial x}\left[C(x)\left(ik_z E_x - \frac{\partial E_z}{\partial x}\right)\right], \tag{14c}$$

$$\frac{\partial E_x}{\partial u} = \frac{\partial}{\partial x}[D(x)E_x] - i\kappa\mu H_z + \frac{i}{\kappa\epsilon}\frac{\partial}{\partial x}\left[C(x)\left(ik_z H_x - \frac{\partial H_z}{\partial x}\right)\right], \tag{14d}$$

where E_z, H_z, E_x, and H_x, as functions of x and u, are the covariant components of the electric and magnetic fields along $\hat{z}$ and $\hat{x}$, respectively. In order to solve these coupled equations, we expand the field amplitudes into Fourier series:

$$\Phi(x, u) = \sum_{m=-\infty}^{\infty} \Phi_m(u)\exp(i\alpha_m x), \tag{15}$$

where Φ stands for any of the four covariant field components. Substitution of these Fourier expansions and the expansions in Eqs. (7) and (8) into Eqs. (14) yields

$$\frac{1}{i}\frac{\mathrm{d}}{\mathrm{d}u} F = MF, \tag{16}$$

where

$$M = \begin{bmatrix} D_{m-n}\alpha_n & \frac{\tau_3}{\tau_1} C_{m-n}\alpha_n & -\frac{1}{\tau_1} C_{m-n} & 0 \\ -\frac{\tau_3}{\tau_2} C_{m-n}\alpha_n & D_{m-n}\alpha_n & 0 & \frac{1}{\tau_2} C_{m-n} \\ \frac{1}{i\mu}(k^2\delta_{mn} - \alpha_m C_{m-n}\alpha_n) & 0 & \alpha_m D_{m-n} & \frac{\tau_3}{\tau_2}\alpha_m C_{m-n} \\ 0 & -\frac{1}{i\epsilon}(k^2\delta_{mn} - \alpha_m C_{m-n}\alpha_n) & -\frac{\tau_3}{\tau_1}\alpha_m C_{m-n} & \alpha_m D_{m-n} \end{bmatrix}, \tag{17}$$

with $m \in U$ and $n \in U$, and, in a form similar to that of Eq. (9), the F vector in a curved medium is defined by

$$F(u) = \left(E_{zm}, H_{zm}, \frac{\kappa}{i} H_{xm}, \frac{\kappa}{i} E_{xm}\right)^T. \tag{18}$$

A solution of Eq. (16) corresponding to an eigenvalue λ_q of M can be written as

$$f_q = \zeta_q \exp(i\lambda_q u) b_q, \tag{19}$$

where ζ_q is the eigenvector of M associated with λ_q, $q \in V$, and b_q is an arbitrary constant. I will call the eigensolution (19) a quasi-Rayleigh wave (or mode). This name is appropriate because, if Eq. (16) were solved with $N \to \infty$, λ_q with a finite q would be nothing but β_m or $-\beta_m$ with an appropriate m and f_q would be the mth term in the usual Rayleigh expansion. [However, the exact solutions to Eq. (16) should not be used in the numerical implementation of the C method.[6,8]] From Eq. (19) the general solution of Eq. (16) can be written in a form similar to that of Eq. (10):

$$F(u) = W\phi(u - u')W^{-1}F(u'), \tag{20}$$

where W is the matrix formed by juxtaposition of ζ_q ($q \in V$),

$$\phi(u) = \delta_{pq} \exp(i\lambda_q u), \tag{21}$$

with δ_{pq} being the Kronecker δ symbol, and u' is an arbitrary constant.

C. Field in the Outermost Media

Here it is assumed that $L \neq 0$ and $P \neq 0$, i.e., the two semi-infinite media are bound by planar interfaces. In terms of the Rayleigh amplitudes for the z components of incident and diffracted waves, the F vector evaluated at the outermost planar interfaces can be written as

$$F^{(L+1)}[y^{(L)}] = W^{(L+1)}[\tilde{R}_n^{(e)}, \tilde{R}_n^{(h)}, \tilde{I}_n^{(e)}, \tilde{I}_n^{(h)}]^T, \tag{22a}$$

$$F^{(P-1)}[y^{(P)}] = W^{(P-1)}[\tilde{J}_n^{(e)}, \tilde{J}_n^{(h)}, \tilde{T}_n^{(e)}, \tilde{T}_n^{(h)}]^T, \tag{22b}$$

where the W matrices are given by Eq. (12) and

$$\begin{aligned} \tilde{R}_n^{(s)} &= R_n^{(s)} \exp[i\beta_n^{(L+1)} y^{(L)}], \\ \tilde{I}_n^{(s)} &= I_n^{(s)} \exp[-i\beta_n^{(L+1)} y^{(L)}], \end{aligned} \tag{23a}$$

$$\begin{aligned} \tilde{J}_n^{(s)} &= J_n^{(s)} \exp[i\beta_n^{(P-1)} y^{(P)}], \\ \tilde{T}_n^{(s)} &= T_n^{(s)} \exp[-i\beta_n^{(P-1)} y^{(P)}]. \end{aligned} \tag{23b}$$

D. Field in the Transition Media

In the original study of Chandezon *et al.* it was assumed that $L = P = 0$, i.e., the two semi-infinite media were bound below and above by the top and bottom corrugated grating surfaces, respectively. One of the novelties of their study was to compose the field in the semi-infinite regions in two distinctive parts, the first part consisting of the incident and propagating diffracted waves, both expressed as the usual Rayleigh expansions, and the second part consisting of the quasi-Rayleigh waves that decay exponentially away from the grating. Popov and Mashev[15] considered grating geometries that had the lower transition layer ($P \neq 0$). They expressed the field in the transition layer solely in terms of the quasi-Rayleigh waves. In the present paper I choose to express the field in both transition media as superpositions of the propagating Rayleigh waves and the decaying quasi-Rayleigh waves away from the corrugated surface and of the propagating and growing Rayleigh waves toward the corrugated surface. This approach, being a natural extension of that of Chandezon *et al.*, has the advantage that it treats the transition layers in a unified way regardless of whether the transition media are finite or semi-infinite.

By writing the field in the lower transition layer as the superpositions as described above, one can derive an equation that relates the F vector in the Cartesian coordinate system to the F vector in the curvilinear coordinate system:

$$F_0(u) = Z_f^{(-1)} \phi^{(-1)}(u - y) Z_g^{(-1)-1} F^{(-1)}(y), \tag{24}$$

where the matrices $Z_f^{(-1)}$ and $Z_g^{(-1)}$ are defined in Appendix A and

$$\begin{aligned} \phi^{(-1)}(\eta) = \exp[+i\beta_m^{(-1)}\eta] \oplus \exp[+i\beta_{m'}^{(-1)}\eta] \oplus \exp[-i\beta_{m'}^{(-1)}\eta] \\ \oplus \exp[-i\beta_{m'}^{(-1)}\eta] \oplus \exp[i\lambda_q^{(-1)}\eta], \end{aligned} \tag{25}$$

with η being a dummy argument, $m' \in U^{(-1)}$, and $q \in V^{(-1)}$. If $P = 0$, then

$$F_0(u = y_0) = Z_f^{(-1)}[\tilde{J}_m^{(e)}, \tilde{J}_m^{(h)}, \tilde{T}_{m'}^{(e)}, \tilde{T}_{m'}^{(h)}, \tilde{b}_q^{(-1)}]^T, \tag{26}$$

where $\tilde{J}_n^{(s)}$ and $\tilde{T}_n^{(s)}$ are given by Eqs. (23b), with $y^{(P)}$ replaced by y_0, and $\tilde{b}_q^{(-1)} = b_q^{(-1)} \exp[i\lambda_q^{(-1)} y_0]$.

Similarly, for the field in the upper transition layer, the following equations can be derived:

$$F^{(+1)}(y) = Z_g^{(+1)} \phi^{(+1)}(y - u) Z_f^{(+1)-1} F_{Q+1}(u), \tag{27}$$

where the matrices $Z_f^{(+1)}$ and $Z_g^{(+1)}$ are defined in Appendix A and

$$\begin{aligned} \phi^{(+1)}(\eta) = \exp[+i\beta_{m'}^{(+1)}\eta] \oplus \exp[+i\beta_{m'}^{(+1)}\eta] \oplus \exp[i\lambda_q^{(+1)}\eta] \\ \oplus \exp[-i\beta_m^{(+1)}\eta] \oplus \exp[-i\beta_m^{(+1)}\eta], \end{aligned} \tag{28}$$

with $m' \in U^{(+1)}$ and $q \in V^{(+1)}$. If $L = 0$, then

$$F_{Q+1}(u = y_Q) = Z_f^{(+1)}[\tilde{R}_{m'}^{(e)}, \tilde{R}_{m'}^{(h)}, \tilde{b}_q^{(+1)}, \tilde{I}_m^{(e)}, \tilde{I}_m^{(h)}]^T, \tag{29}$$

where $\tilde{R}_n^{(s)}$ and $\tilde{I}_n^{(s)}$ are given by Eqs. (23a), with $y^{(L)}$ replaced by y_Q, and $\tilde{b}_q^{(+1)} = b_q^{(+1)} \exp[i\lambda_q^{(+1)} y_Q]$.

E. System of Linear Equations

The ultimate task of all rigorous grating methods, including the C method, is to construct and then solve a system of linear equations of the form

$$AX = b, \tag{30}$$

where A is a square matrix, b is a column vector containing the incident wave, and X is a column vector representing the unknown Rayleigh amplitudes in the two outermost media. Although vector X is uniquely defined once an incident wave is given and a truncation order is chosen, matrix A and vector b may take vastly different forms depending on the mathematical methods and numerical algorithms that have been used in their derivation.

Since, in the C method, the coordinate surfaces $y = y^{(j)}$ and $u = y_j$ coincide with the planar and curved medium interfaces, respectively, the Cartesian field components E_x and H_x at the planar interfaces and the covariant components E_x and H_x at the curved interfaces are tangent to their respective medium interfaces. Thus the field-matching conditions across all the medium interfaces are simply the continuities of the F vectors. It then follows from the results in the previous subsections that, for $L \geq 2$, $P \leq -2$, and $Q \geq 1$,

$$W^{(L+1)}[\tilde{R}_n^{(e)}, \tilde{R}_n^{(h)}, \tilde{I}_n^{(e)}, \tilde{I}_n^{(h)}]^T = TW^{(P-1)}[\tilde{J}_n^{(e)}, \tilde{J}_n^{(h)}, \tilde{T}_n^{(e)}, \tilde{T}_n^{(h)}]^T, \tag{31}$$

with

$$T = \left\{\prod_{j=2}^{L} W^{(j)}\phi^{(j)}[e^{(j)}]W^{(j)-1}\right\}\{Z_g^{(+1)}\phi^{(+1)}[e^{(+1)}]Z_f^{(+1)-1}\} \times \left[\prod_{j=1}^{Q} W_j\phi_j(e_j)W_j^{-1}\right]\{Z_f^{(-1)}\phi^{(-1)}[e^{(-1)}]Z_g^{(-1)-1}\} \times \left\{\prod_{j=P}^{-2} W^{(j)}\phi^{(j)}[e^{(j)}]W^{(j)-1}\right\}, \tag{32}$$

where the consecutive factors under the multiplication signs are appended from the left-hand side to the products. If $L = P = 0$ and $Q \neq 0$, which is the case investigated by Chandezon *et al.*, then the above two equations are replaced by

$$Z_f^{(+1)}[\tilde{R}_{n'}^{(e)}, \tilde{R}_{n'}^{(h)}, \tilde{b}_q^{(+1)}, \tilde{I}_n^{(e)}, \tilde{I}_n^{(h)}]^T = TZ_f^{(-1)}[\tilde{J}_m^{(e)}, \tilde{J}_m^{(h)}, \tilde{T}_{m'}^{(e)}, \tilde{T}_{m'}^{(h)}, \tilde{b}_p^{(-1)}]^T, \tag{33}$$

with

$$T = \prod_{j=1}^{Q} W_j\phi_j(e_j)W_j^{-1}, \tag{34}$$

where $m' \in U^{(-1)}$, $n' \in U^{(+1)}$, $p \in V^{(-1)}$, and $q \in V^{(+1)}$. The equivalent equations for other combinations of the values of L, P, and Q can be derived similarly.

In principle, the solution to the grating problem is completed at this point. Indeed, as in Refs. 6, 9, and 10, a system of linear equations of type (30) can be derived from Eq. (31) or (33) and solved with a standard numerical technique. In practice, however, it turns out to be a nontrivial matter as to how the linear system is derived when a finite word-length computer is used.

4. IMPROVEMENTS TO THE C METHOD

A. Application of the *R*-Matrix Propagation Algorithm

The numerical difficulties that Chandezon *et al.* experienced with gratings having a large number of coated layers or a large total thickness were actually not caused by the precision problems in the evaluation of the eigenvalues and the eigenvectors; they were caused by the method that was used in the derivation of the system of linear equations. For a high-order Rayleigh wave or quasi-Rayleigh wave the magnitude of the imaginary part of the eigenvalue β or λ can be a large number. Thus very large and very small (relative to the computer's word length) exponential terms may appear simultaneously in a diagonal matrix ϕ. When one uses a computer to evaluate the matrix product in Eq. (32) or (34), these exponential terms may cause severe loss of significant digits in the numerical values of the T-matrix elements. For example, it can be shown that theoretically the determinant of the matrix product in Eq. (34) is unity for a dielectric coated grating, but the numerically evaluated matrix product may be singular if the number of layers is high or the total thickness is large. The situation here is exactly the same as the situation in which the classical modal method was used to treat arbitrary grating profiles by the use of the multilayer approximation.[1] There the R-matrix propagation algorithm was used with spectacular success to remove numerical instabilities that occurred for deep gratings. This algorithm can be used here without any change.

In preparation for the application of the R-matrix propagation algorithm the T matrix must be factored such that

$$T = \prod_{l=1}^{l'} t^{(l)}, \tag{35}$$

where l' is an integer and the $t^{(l)}$, to be defined below, are called the sector t matrices. With this factorization Eqs. (31) and (32) or (33) and (34) are equivalent to the recursion formula

$$\begin{pmatrix}\Omega_l \\ X_l\end{pmatrix} = t^{(l)}\begin{pmatrix}\Omega_{l-1} \\ X_{l-1}\end{pmatrix}, \tag{36}$$

provided that the column vector $(\Omega_0{}^T, X_0{}^T)^T$ is the column vector on the right-hand side of matrix T in Eq. (31) or (33) and that the column vector $(\Omega_{l'}{}^T, X_{l'}{}^T)^T$ is the column vector on the left-hand side of Eq. (31) or (33). In the R-matrix propagation algorithm Eq. (36) is transformed into a different form,

$$\begin{pmatrix}\Omega_{l-1} \\ \Omega_l\end{pmatrix} = r^{(l)}\begin{pmatrix}X_{l-1} \\ X_l\end{pmatrix}, \tag{37}$$

where $r^{(l)}$ is called the sector r matrix and is related to $t^{(l)}$ in a 2×2 block form by

$$\begin{bmatrix} r_{11}^{(l)} & r_{12}^{(l)} \\ r_{21}^{(l)} & r_{22}^{(l)} \end{bmatrix} = \begin{bmatrix} -t_{21}^{(l)-1}t_{22}^{(l)} & t_{21}^{(l)-1} \\ t_{12}^{(l)} - t_{11}^{(l)}t_{21}^{(l)-1}t_{22}^{(l)} & t_{11}^{(l)}t_{21}^{(l)-1} \end{bmatrix}. \tag{38}$$

Furthermore, the global R matrices are introduced by

$$\begin{pmatrix}\Omega_0\\ \Omega_l\end{pmatrix} = R^{(l)}\begin{pmatrix}X_0\\ X_l\end{pmatrix}. \tag{39}$$

It can be shown that the 2×2 blocks of the R matrices obey the recursion formulas

$$\begin{aligned} R_{11}^{(l)} &= R_{11}^{(l-1)} + R_{12}^{(l-1)} Z^{(l)} R_{21}^{(l-1)},\\ R_{12}^{(l)} &= -R_{12}^{(l-1)} Z^{(l)} r_{12}^{(l)},\\ R_{21}^{(l)} &= r_{21}^{(l)} Z^{(l)} R_{21}^{(l-1)},\\ R_{22}^{(l)} &= r_{22}^{(l)} - r_{21}^{(l)} Z^{(l)} r_{12}^{(l)}, \end{aligned} \tag{40}$$

where

$$Z^{(l)} = [r_{11}^{(l)} - R_{22}^{(l-1)}]^{-1}. \tag{41}$$

The recursion can be initialized by $R^{(1)} = r^{(1)}$ or, if only the reflected diffraction orders are to be determined, by $R^{(0)} = W_{22}^{(P-1)-1} \oplus W_{22}^{(P-1)-1}$ when Eq. (31) is used and by $R^{(0)} = Z_{f12}^{(-1)} Z_{f22}^{(-1)-1} \oplus Z_{f12}^{(-1)} Z_{f22}^{(-1)-1}$ when Eq. (33) is used, where 12 and 22 denote the blocks of the matrices written in a 2×2 block form. After the R-matrix propagation is completed with the above recursion scheme, a system of linear equations of type (30) can be derived from Eq. (39) with $l = l'$.

The factorization of the T matrix is not unique, but it is also not completely arbitrary. Apart from the obvious requirement that the 21 block of each t matrix be invertible, there is a subtlety that the reader should be made aware of. Suppose that the T matrix is defined by Eq. (34). Then it seems natural to define the sector t matrices such that $t^{(j)} = W_j \phi_j W_j^{-1}$. However, a computer program that I built based on this factorization scheme was unable to produce correct diffraction efficiency values if any of the coated layers is thicker than approximately half of a wavelength, although it performed well for gratings having dozens of coated layers less than this thickness. Here again it was the exponential factor that was causing the numerical difficulties—the loss of significant digits already occurred in the construction of the individual sector t matrices before they were converted to the sector r matrices.

The remedy for the problem is to factor the T matrix such that each t matrix either contains no ϕ matrix or has it exposed on one side, for example the left-hand side. For the T matrix given by Eq. (34) the following factorization seems to be a good choice:

$$T = W_Q \prod_{j=2}^{Q} [\phi(e_j) W_j^{-1} W_{j-1}] \phi(e_1) W_1^{-1}. \tag{42}$$

Let us see how it works. With the layer-identifying subscripts omitted, a typical sector t matrix in Eq. (42) takes the form

$$t = \begin{bmatrix} \exp(i\lambda_m^+ e) & 0 \\ 0 & \exp(i\lambda_m^- e) \end{bmatrix} \begin{bmatrix} A_{11} & A_{12} \\ A_{21} & A_{22} \end{bmatrix}, \tag{43}$$

where λ_m^+ and λ_m^- denote the eigenvalues of matrix M with nonnegative and nonpositive imaginary parts, respectively. It will be shown in Subsection 4.B that such a division of the eigenvalues is always possible for a lossless dielectric layer, regardless of the grating profile, or for a symmetrical grating profile, regardless of the permittivity. If the grating profile is asymmetrical and the medium is lossy, the division of the eigenvalues also appears always possible because, as numerical experiments show, the numbers of eigenvalues with positive and negative imaginary parts are always equal, although it is not clear if this assertion can be mathematically proven. Application of the transformation rule (38) to this t matrix gives

$$r = \begin{bmatrix} -A_{21}^{-1} A_{22} & A_{21}^{-1} \exp(-i\lambda^- e) \\ \exp(i\lambda^+ e)(A_{12} - A_{11} A_{21}^{-1} A_{22}) & \exp(i\lambda^+ e) A_{11} A_{21}^{-1} \exp(-i\lambda^- e) \end{bmatrix}. \tag{44}$$

It is evident that the magnitudes of the exponential factor in this sector r matrix are all decreasing functions of the layer thickness and the eigenvalue order number; therefore the catastrophic loss of significant digits that would have happened if the ϕ matrix were sandwiched between two W matrices has been avoided.

In summary, while the R-matrix propagation algorithm provides the improved C method with robustness in dealing with a large number of layers, the delicate construction of the sector r matrix in Eq. (44) ensures its numerical stability for large thickness of the individual layers. When the R-matrix propagation algorithm is properly implemented, a computer program based on the improved C method should produce convergent results without any of the numerical difficulties that have been experienced by earlier authors regarding the total layer thickness and the total number of layers.

B. Use of the Symmetry Properties of the Eigenvalue Problem

1. *Symmetry Properties of the Eigenvalue Problem*

The algebraic eigenvalue problem associated with the matrix M that is defined in Eq. (17) has many interesting symmetry properties that, when they are fully applied, can lead to significant reduction of numerical computation in the C method. Although the symmetry properties of the counterpart of M in the nonconical mounts were studied by Chandezon,[16] they were not fully exploited for numerical purposes. The symmetry properties of M in the conical mountings, on the other hand, have not been reported at all in the literature. The use of the symmetry properties of M is detailed in the Subsections 4.B.2 and 4.B.3. In this subsection I enumerate the known symmetry properties that are independent of the incident angle and the matrix truncation. The following statements are given without proof. The interested reader can easily verify them by using elementary matrix manipulations, such as row and column exchanges and multiplications by scalars, on matrix M and by using the symmetry properties of the Fourier coefficients C_m and D_m given in Eqs. (7) and (8). Throughout Subsection 4.B the medium-identifying subscripts are omitted.

Polarization Degeneracy. Regardless of the grating profile and the medium permittivity, for every eigenvector $(\nu_{1m}, \nu_{2m}, \nu_{3m}, \nu_{4m})^T$ of M associated with the eigenvalue λ there is another eigenvector $[(-\mu/\epsilon)\nu_{2m}, \nu_{1m}, (-\mu/\epsilon)\nu_{4m}, \nu_{3m}]^T$ of M associated with

the same λ. Thus every eigenvalue of M is at least doubly degenerate. The reason for calling this degeneracy the polarization degeneracy will be made clear in Subsection 4.B.2.

Reflection Symmetry. Assuming that the medium is lossless, then, regardless of the grating profile, if λ is an eigenvalue of M, so is $\bar{\lambda}$, where the bar indicates complex conjugation (a reflection with respect to the real axis of the complex plane). Furthermore, if $(\nu_{1m}, \nu_{2m}, \nu_{3m}, \nu_{4m})^T$ is a (right) eigenvector of M associated with λ, then $(\nu_{3m}, -\nu_{4m}, -\nu_{1m}, \nu_{2m})^T$ is a left eigenvector[14] of M associated with $\bar{\lambda}$, i.e., it is a (right) eigenvector of M^* associated with λ.

Reversal Symmetry. Assuming that the grating profile is symmetrical, then, regardless of the medium permittivity, if λ is an eigenvalue of M, so is $-\lambda$ (a simultaneous sign reversal of both the real and imaginary parts). Furthermore, if $(\nu_{1m}, \nu_{2m}, \nu_{3m}, \nu_{4m})^T$ is a (right) eigenvector of M associated with λ, then $(-\bar{\nu}_{3m}, -\bar{\nu}_{4m}, \bar{\nu}_{1m}, \bar{\nu}_{2m})^T$ is a left eigenvector of M associated with $-\lambda$, i.e., it is a (right) eigenvector of M^* associated with $-\bar{\lambda}$.

2. Use of the Polarization Degeneracy

It seems that the numerical work in solving the eigenvalue problem in the conical mountings can be reduced by half because, according to the polarization degeneracy, if $2N$ eigenvectors corresponding to $2N$ distinctive eigenvalues are numerically determined, the other $2N$ eigenvectors can be obtained analytically. However, for a general eigenvalue problem solver, it takes as much time to obtain half of the eigensolutions as to obtain all the eigensolutions. Thus the polarization degeneracy cannot be taken advantage of by the direct use of matrix M. However, a careful analysis of Eqs. (14), from which matrix M is derived, offers a much better solution.

It follows from Eqs. (14a) and (14b) that the x components of the field can be expressed in terms of the z components:

$$E_x = -\frac{\tau_2}{\kappa}\left[\dot{a}\frac{\partial H_z}{\partial x} - (1+\dot{a}^2)\frac{\partial H_z}{\partial u}\right] + \frac{\tau_3}{\kappa}\frac{\partial E_z}{\partial x}, \quad (45a)$$

$$H_x = \frac{\tau_1}{\kappa}\left[\dot{a}\frac{\partial E_z}{\partial x} - (1+\dot{a}^2)\frac{\partial E_z}{\partial u}\right] + \frac{\tau_3}{\kappa}\frac{\partial H_z}{\partial x}. \quad (45b)$$

Substitution of these two expressions into Eqs. (14c) and (14d) yields two equations of identical form involving the z components only:

$$\left[\frac{\partial^2}{\partial x^2} + (1+\dot{a}^2)\frac{\partial^2}{\partial u^2} - 2\dot{a}\frac{\partial^2}{\partial x \partial u} - \ddot{a}\frac{\partial}{\partial u} + \tilde{k}^2\right]\begin{pmatrix} E_z \\ H_z \end{pmatrix} = \begin{pmatrix} 0 \\ 0 \end{pmatrix}. \quad (46)$$

It is tacitly understood that these equations are to be solved subject to the pseudoperiodic condition. When Fourier expansions are used for all the x dependencies, Eq. (46) is fully equivalent to Eq. (16). In the C method Eq. (16) is solved instead of Eq. (46) because it yields an easier numerical solution. However, Eq. (46) reveals certain characteristics of the eigenvalue problem that are concealed by Eq. (16). These characteristics, to be described below, lead to significant reduction of computational effort for gratings in conical mountings.

The fact that E_z and H_z are uncoupled means that there are two types of solution to Eqs. (14): the $H_\perp$ type for which $H_z = 0$ and the $E_\perp$ type for which $E_z = 0$. Clearly, when $k_z = 0$, the $H_\perp$ type corresponds to the TE polarization and the $E_\perp$ type corresponds to the TM polarization. From Eqs. (45) the $H_\perp$- and $E_\perp$-type F vectors can be easily obtained:

$$F^{(e)} = \begin{pmatrix} E_{zm}^{(e)} \\ 0 \\ -i\tau_1\left[\dot{a}\frac{\partial E_z^{(e)}}{\partial x} - (1+\dot{a}^2)\frac{\partial E_z^{(e)}}{\partial u}\right]_m \\ \tau_3 \alpha_m E_{zm}^{(e)} \end{pmatrix}, \quad (47a)$$

$$F^{(h)} = \begin{pmatrix} 0 \\ H_{zm}^{(h)} \\ \tau_3 \alpha_m H_{zm}^{(h)} \\ i\tau_2\left[\dot{a}\frac{\partial H_z^{(h)}}{\partial x} - (1+\dot{a}^2)\frac{\partial H_z^{(h)}}{\partial u}\right]_m \end{pmatrix}. \quad (47b)$$

Since E_z and H_z satisfy the identical equation and the pseudoperiodic condition, they share the same eigenvalues. For a given eigenvalue the eigenvectors given by Eqs. (47a) and (47b) are clearly linearly independent; hence the name polarization degeneracy. For the same reason mentioned above, E_z and H_z also share the same functional form; therefore the two F vectors in Eqs. (47a) and (47b) are determined by only one function, $E_z^{(e)}$ for example.

A reader who is familiar with the results of Chandezon *et al.* may have recognized that Eq. (46) is exactly the same as Eq. (7) in Ref. 8, provided that k^2 is replaced by $\tilde{k}^2$. Therefore the eigenvalues and the eigenfunctions E_z and H_z of Eqs. (46) in a conical mount can be obtained as solutions to the same equations but in the corresponding induced nonconical mount (defined in Section 2) in one of the two fundamental polarizations, for example the TE polarization. Suppose that $f = E_z$ and $g = (\kappa/i)H_x$ in the induced nonconical mount; then[6,8]

$$\frac{1}{i}\frac{\mathrm{d}}{\mathrm{d}u}\begin{pmatrix} f_m \\ g_m \end{pmatrix} = M'\begin{pmatrix} f_m \\ g_m \end{pmatrix}, \quad (48)$$

where

$$M' = \begin{bmatrix} D_{m-n}\alpha_n & i\mu C_{m-n} \\ \frac{1}{i\mu}(\tilde{k}^2\delta_{mn} - \alpha_m C_{m-n}\alpha_n) & \alpha_m D_{m-n} \end{bmatrix}. \quad (49)$$

Once Eq. (48) is solved numerically, both f and g are determined. On the other hand, from Eq. (45b) with $k_z = 0$,

$$g_m = \frac{1}{\mu}\left[\dot{a}\frac{\partial f}{\partial x} - (1+\dot{a}^2)\frac{\partial f}{\partial u}\right]_m. \quad (50)$$

On substitution of f for $E_z^{(e)}$ and $H_z^{(h)}$ in Eqs. (47a) and (47b), respectively, the F vectors of both $H_\perp$ and $E_\perp$ types can be written in terms of f and g:

$$F^{(e)} = \begin{pmatrix} f_m \\ 0 \\ -i\tau_1 \mu g_m \\ \tau_3 \alpha_m f_m \end{pmatrix}, \qquad F^{(h)} = \begin{pmatrix} 0 \\ f_m \\ \tau_3 \alpha_m f_m \\ i\tau_2 \mu g_m \end{pmatrix}. \tag{51}$$

In this subsection the u-dependent F vectors have been the subject of discussion. However, it is not difficult to see that the conclusions that have been reached here apply to the eigenvectors of matrix M as well. In particular, Eqs. (51) give two eigenvectors of M if $(f_m, g_m)^T$ is taken as the eigenvector of matrix M'.

In summary, the eigensolutions of matrix M for a grating in a conical mount can be obtained by solution of the eigenvalue problem of matrix M' for the induced nonconical mount. The $2N$ eigenvalues of M' give the $4N$ eigenvalues of M, each of them being doubly degenerate, and each eigenvector of M' generates two eigenvectors of M by Eqs. (51). The bulk of the execution time (>90%) of a computer program based on the C method is actually consumed by the eigenvalue problem solver, and this amount of time is roughly proportional to the cube of the matrix dimension. Since matrix M' is only half the size of matrix M, the procedure described above greatly reduces the computation time of the C method. I performed some experiments with two nearly identical computer programs based on the C method. When modeling gratings in conical mountings, the one that employed the procedure to take advantage of the polarization degeneracy ran approximately four to five times faster than the one that did not.

3. Use of the Reflection and Reversal Symmetries

The reflection and reversal symmetries also find applications in the numerical implementation of the C method. When $Q > 0$, the inverse matrices ${W_j}^{-1}$, $j = 1, 2, \ldots, Q$, appear in the formalism. Of course, one should never compute ${W_j}^{-1}$ separately and then form a matrix product, such as ${W_j}^{-1}W_{j-1}$ in Eq. (42). Instead, the product should be obtained as a solution to the matrix equation $W_j X = W_{j-1}$. Even so, such a numerical procedure is costly, especially when it must be repeated for many coated layers. One can use the reflection and reversal symmetries effectively to construct the inverse matrices ${W_j}^{-1}$ virtually without any numerical computation.

The magic is performed with the aid of the principle of biorthogonality in matrix theory,[17] which says that if M is a square matrix and if λ and μ are its two eigenvalues with $\lambda \neq \mu$, then, for any left eigenvector w of M corresponding to λ and any right eigenvector v of M corresponding to μ, $w^* v = 0$. In the present situation, thanks to the symmetry properties, the left eigenvectors of M are directly obtainable from the right eigenvectors, thus making the construction of the inverse matrix effortless.

In preparation for the construction of W^{-1}, the eigenvalues of M need to be sorted appropriately. In this subsection I restrict the integers p, q, and r to the ranges

$$1 \le p \le N_0 - 1, \qquad N_0 \le q \le N, \qquad 1 \le r \le N, \tag{52}$$

where $N_0 \ge 0$ is one fourth of the number of the real eigenvalues (there are an equal number of positive and negative eigenvalues). The $4N$ eigenvalues of matrix M are ordered in eight blocks as follows:

$$\begin{aligned} &\{\lambda_p^{(e)+}\}, \quad \{\lambda_q^{(e)+}\}, \quad \{\lambda_p^{(h)+}\}, \quad \{\lambda_q^{(h)+}\}, \\ &\{\lambda_p^{(e)-}\}, \quad \{\lambda_q^{(e)-}\}, \quad \{\lambda_p^{(h)-}\}, \quad \{\lambda_q^{(h)-}\}, \end{aligned} \tag{53}$$

where

$$\lambda_p^{(s)\pm} \gtrless 0, \qquad \mathrm{Im}[\lambda_q^{(s)\pm}] \gtrless 0, \tag{54}$$

with the upper signs or the lower signs being taken simultaneously. Of course, because of the polarization symmetry, $\{\lambda_p^{(e)\pm}\} = \{\lambda_p^{(h)\pm}\}$ and $\{\lambda_q^{(e)\pm}\} = \{\lambda_q^{(h)\pm}\}$. Within each block the eigenvalues are ordered such that

$$1 \le a < b \le N_0 - 1 \quad \text{if } \lambda_a^{(s)\pm} \gtrless \lambda_b^{(s)\pm}, \tag{55a}$$

$$N_0 \le a < b \le N \quad \text{if } \mathrm{Im}[\lambda_a^{(s)\pm}] \gtrless \mathrm{Im}[\lambda_b^{(s)\pm}]$$
$$\text{or if } \mathrm{Im}[\lambda_a^{(s)\pm}] = \mathrm{Im}[\lambda_b^{(s)\pm}] \text{ and } \mathrm{Re}[\lambda_a^{(s)\pm}] < \mathrm{Re}[\lambda_b^{(s)\pm}]. \tag{55b}$$

With this ordering the W matrix can be written in a 4×8 block form:

$$W = \begin{bmatrix} \nu_{1p}^{(e)+} & \nu_{1q}^{(e)+} & \nu_{1p}^{(h)+} & \nu_{1q}^{(h)+} & \nu_{1p}^{(e)-} & \nu_{1q}^{(e)-} & \nu_{1p}^{(h)-} & \nu_{1q}^{(h)-} \\ \nu_{2p}^{(e)+} & \nu_{2q}^{(e)+} & \nu_{2p}^{(h)+} & \nu_{2q}^{(h)+} & \nu_{2p}^{(e)-} & \nu_{2q}^{(e)-} & \nu_{2p}^{(h)-} & \nu_{2q}^{(h)-} \\ \nu_{3p}^{(e)+} & \nu_{3q}^{(e)+} & \nu_{3p}^{(h)+} & \nu_{3q}^{(h)+} & \nu_{3p}^{(e)-} & \nu_{3q}^{(e)-} & \nu_{3p}^{(h)-} & \nu_{3q}^{(h)-} \\ \nu_{4p}^{(e)+} & \nu_{4q}^{(e)+} & \nu_{4p}^{(h)+} & \nu_{4q}^{(h)+} & \nu_{4p}^{(e)-} & \nu_{4q}^{(e)-} & \nu_{4p}^{(h)-} & \nu_{4q}^{(h)-} \end{bmatrix}, \tag{56}$$

where the subscripts identify the eigenvalues with which the eigenvectors are associated and, for simplicity, the subscript m in $\nu_{1p}^{(s)\pm} = \nu_{1mp}^{(s)\pm}$, etc., has been omitted.

In the following I assume that the spectrum of M does not have any degeneracies other than the polarization degeneracy. Then it is easy to verify that, for a lossless coated layer,

$$\tilde{W}^{-1} W = D, \tag{57}$$

where D is a diagonal matrix, and

$$\tilde{W}^{-1} = \begin{bmatrix} \nu_{3p}^{(e)+} & \nu_{3q}^{(e)-} & \nu_{3p}^{(h)+} & \nu_{3q}^{(h)-} & \nu_{3p}^{(e)-} & \nu_{3q}^{(e)+} & \nu_{3p}^{(h)-} & \nu_{3q}^{(h)+} \\ -\nu_{4p}^{(e)+} & -\nu_{4q}^{(e)-} & -\nu_{4p}^{(h)+} & -\nu_{4q}^{(h)-} & -\nu_{4p}^{(e)-} & -\nu_{4q}^{(e)+} & -\nu_{4p}^{(h)-} & -\nu_{4q}^{(h)+} \\ -\nu_{1p}^{(e)+} & -\nu_{1q}^{(e)-} & \nu_{1p}^{(h)+} & -\nu_{1q}^{(h)-} & -\nu_{1p}^{(e)-} & -\nu_{1q}^{(e)+} & -\nu_{1p}^{(h)-} & -\nu_{1q}^{(h)+} \\ \nu_{2p}^{(e)+} & \nu_{2q}^{(e)-} & \nu_{2p}^{(h)+} & \nu_{2q}^{(h)-} & \nu_{2p}^{(e)-} & \nu_{2q}^{(e)+} & \nu_{2p}^{(h)-} & \nu_{2q}^{(h)+} \end{bmatrix}^*. \tag{58}$$

It can be safely assumed that all the diagonal elements of D are nonzero because the converse case is extremely rare. Therefore the inverse of matrix W is given by

$$W^{-1} = D^{-1}\tilde{W}^{-1}. \tag{59}$$

Essentially, the purpose of matrix multiplication above is to normalize the left eigenvectors with respect to the corresponding right eigenvectors. For gratings with a symmetrical groove profile Eqs. (57) and (59) are still valid provided that

$$\tilde{W}^{-1} = \begin{bmatrix} -\nu_{3r}^{(e)-} & -\nu_{3r}^{(h)-} & -\nu_{3r}^{(e)+} & -\nu_{3r}^{(h)+} \\ -\nu_{4r}^{(e)-} & -\nu_{4r}^{(h)-} & -\nu_{4r}^{(e)+} & -\nu_{4r}^{(h)+} \\ \nu_{1r}^{(e)-} & \nu_{1r}^{(h)-} & \nu_{1r}^{(e)+} & \nu_{1r}^{(h)+} \\ \nu_{2r}^{(e)-} & \nu_{2r}^{(h)-} & \nu_{2r}^{(e)+} & \nu_{2r}^{(h)+} \end{bmatrix}^T. \tag{60}$$

In deriving Eqs. (58) and (60), I have used the fact that the left-hand eigenvector and the right-hand eigenvector of M having different polarizations are always orthogonal regardless of their eigenvalues. It is easy to check that, when both the lossless condition and the symmetry conditions are satisfied, the two matrices defined by Eqs. (58) and (60) are identical.

Besides the polarization degeneracy, matrix M may have additional degeneracies, for example when $\alpha_n = -\alpha_0$ for some n. In this case, instead of being diagonal, matrix D becomes block diagonal. In principle, one can still use Eq. (59) to define W^{-1}. However, since it is difficult to know *a priori* exactly which eigenvalues are degenerate, one must either numerically determine the locations of the nondiagonal blocks and then invert the blocks, which increases the program's complexity, or apply a standard linear system solver to D as a whole. In such an event it may simply be equally cost effective to obtain W^{-1} directly by a numerical technique.

5. REDUCTION TO THE CLASSICAL MOUNT

The mathematical description of the C method has been given in Sections 3 and 4 for the conical mountings. Most vectors and matrices there have been defined in units of $1 \times N$ or $N \times N$ blocks. It is easy to reduce all the equations to the nonconical mountings. Besides setting $k_z = 0$, one needs only to perform matrix contractions. The set of equations for the TE polarization can be obtained if we cross out the second and fourth block rows and block columns of all the vectors and the matrices. Similarly, the set of equations for the TM polarization can be obtained if we cross out the first and third block rows and block columns of all the vectors and the matrices. For example, matrix M' in Eq. (49) was obtained in this way from matrix M in Eq. (17).

6. NUMERICAL EXAMPLES

The convergence of the C method has been investigated by Popov and Mashev.[11,12] As far as bare gratings are concerned, their conclusion should remain valid for the improved C method because the improvements made in Subsection 4.B do not alter the underlying inner working of the C method. On the other hand, their conclusions for coated gratings are likely to be modified significantly because the incorporation of the R-matrix propagation algorithm into the C method has fundamentally changed the way in which the system of linear equations leading to the diffraction efficiencies is derived. However, a detailed convergence study of the improved C method is beyond the scope of this paper.

This section serves two purposes: it provides some tabulated results, which may be useful to a reader who plans to implement the C method, and it provides a few plots to illustrate the effectiveness of the improved C method in dealing with coated gratings.

Tables 1 and 2 include diffraction efficiencies of two bare and two metal-coated sinusoidal dielectric gratings in a conical mount. The first bare grating is identical to one of the gratings considered in Tables 1 and 2 of Ref. 18. Note that the metal coatings are not sufficiently thick, so a small amount of energy is transmitted into the substrate.

In Figs. 3–6 the diffraction efficiencies of sinusoidal dielectric and metallic gratings having large numbers of dielectric coatings of varying thicknesses are plotted. The (vertical) thicknesses ρ_j of the layers are measured in a dimensionless unit, so that

Table 1. Diffraction Efficiencies of Bare and Metal-Coated Sinusoidal Gratings[a]

Propagating Order[b]	Bare		Coated	
	$h/d = 0.1$	$h/d = 0.5$	$h/d = 0.1$	$h/d = 0.5$
R, −3	0.38400(−4)	0.41490(−1)	0.27912(−3)	0.43038
R, −2	0.19458(−2)	0.12816(−1)	0.12472(−1)	0.90097(−1)
R, −1	0.27328(−1)	0.23730(−1)	0.14003	0.18422
R, 0	0.26590	0.77140(−1)	0.83747	0.26516
T, −5	0.25201(−7)	0.47617(−3)	0.95554(−10)	0.11117(−3)
T, −4	0.10985(−6)	0.28018(−3)	0.24464(−8)	0.23508(−3)
T, −3	0.26059(−4)	0.27595(−1)	0.18432(−6)	0.55610(−3)
T, −2	0.24662(−2)	0.71698(−1)	0.48483(−5)	0.21567(−2)
T, −1	0.63581(−1)	0.17254	0.56180(−4)	0.13404(−2)
T, 0	0.49256	0.18548	0.72484(−3)	0.25958(−2)
T, +1	0.14375	0.29541	0.29416(−3)	0.58921(−2)
T, +2	0.24006(−2)	0.91346(−1)	0.95765(−5)	0.20947(−2)

[a] $\xi = 15°$, $\theta = 60°$, $d/\lambda = 2$, $n^{(+1)} = 1$, $n^{(-1)} = 2$, $n_1 = 0.1 + i5.0$, $e_1/\lambda = 0.1$, and $I_z^{(h)} = 0$. The integers in parentheses are base 10 exponents.
[b] R, Reflected order; T, transmitted order.

Table 2. Diffraction Efficiencies of Bare and Metal-Coated Sinusoidal Gratings[a]

Propagating Order	Bare		Coated	
	$h/d = 0.1$	$h/d = 0.5$	$h/d = 0.1$	$h/d = 0.5$
R, −3	0.70629(−4)	0.55051(−1)	0.91872(−3)	0.40090
R, −2	0.24214(−2)	0.50608(−2)	0.31398(−1)	0.19947
R, −1	0.14349(−1)	0.38300(−2)	0.26107	0.21474
R, 0	0.55655(−2)	0.49169(−2)	0.67563	0.12491
T, −5	0.54483(−7)	0.31483(−3)	0.12272(−8)	0.72505(−3)
T, −4	0.55487(−7)	0.59471(−2)	0.33424(−7)	0.81708(−3)
T, −3	0.57954(−4)	0.68862(−1)	0.22882(−5)	0.36651(−2)
T, −2	0.40853(−2)	0.14226	0.46324(−4)	0.10160(−2)
T, −1	0.96658(−1)	0.14008	0.38754(−3)	0.81983(−2)
T, 0	0.71283	0.14560	0.24476(−2)	0.37013(−3)
T, +1	0.16212	0.35949	0.88808(−3)	0.43986(−2)
T, +2	0.18384(−2)	0.68595(−1)	0.65794(−4)	0.50533(−2)

[a]Same as Table 1, except that $I_z^{(e)} = 0$.

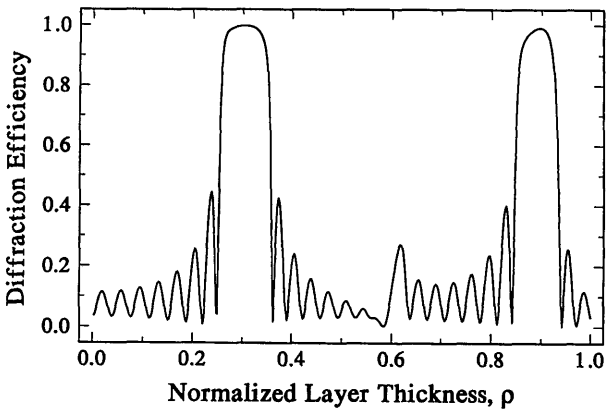

Fig. 3. First-order Littrow mount diffraction efficiency of a coated sinusoidal grating. The parameters are $\lambda = 0.59\ \mu m$, $d = 0.3333\ \mu m$, $h = 0.12\ \mu m$, $Q = 15$, $n^{(+1)} = 1.0$, $n^{(-1)} = 1.46$, $n_j = 2.37$ with odd j, $n_j = 1.35$ with even j, and TM polarization.

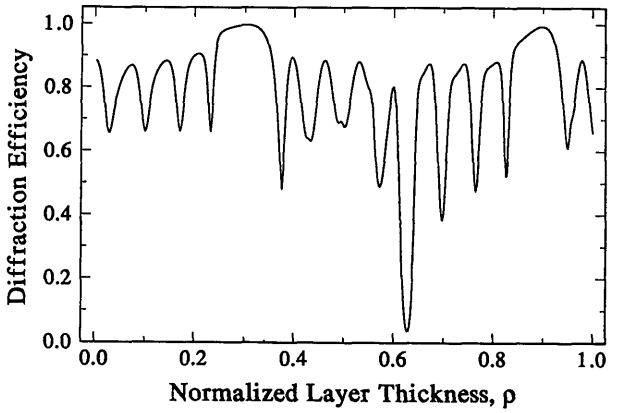

Fig. 4. Same as Fig. 3 except that $n^{(-1)} = 1.15 + i7.15$, $n_j = 2.37$ with even j, $n_j = 1.35$ with odd j, and $Q = 8$.

$$\rho_j = \frac{e_j n_j}{\lambda}, \tag{61}$$

where λ is the vacuum wavelength and $n_j = \sqrt{\epsilon_j}$ is the refractive index. It is assumed in the examples below that all the coated layers have the same normalized thickness ρ. The gratings are used in the TM polarization and, except in Fig. 6, at the first-order Littrow mount.

The first example, shown in Fig. 3, is for a 15-layer-coated silica (SiO_2, $n = 1.46$) grating. The coatings consist of alternating layers of zinc sulfite (ZnS, $n = 2.37$) and cryolite (Na_3AlF_6, $n = 1.35$), with a ZnS layer adjacent to the SiO_2 substrate. All the other parameters are identical to one of the gratings considered in Table 1 of Ref. 19. Note that, although the bare grating's efficiency at the

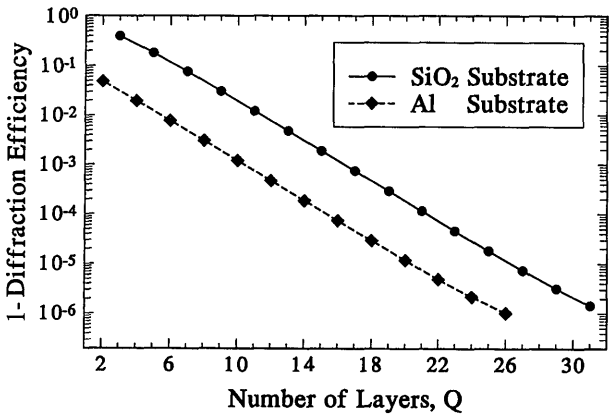

Fig. 5. Dependencies of the peak first-order Littrow mount diffraction efficiencies of the two gratings in Figs. 3 and 4 on the number of coated layers. The normalized thickness is fixed at $\rho = 0.304$.

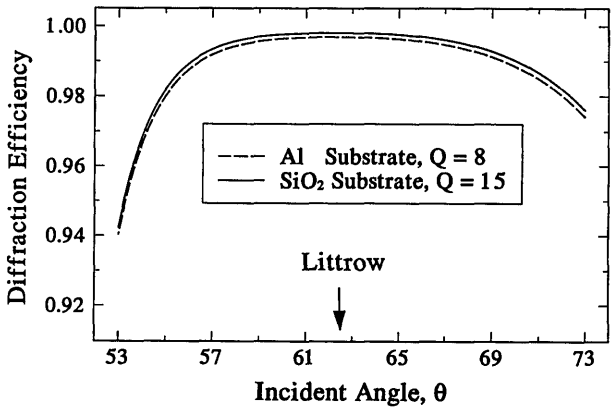

Fig. 6. Angular dependencies of the peak first-order Littrow mount diffraction efficiencies of the two gratings in Figs. 3 and 4. The normalized thickness is fixed at $\rho = 0.304$.

chosen groove depth, $h = 0.12\ \mu$m, is only 3.3%, the efficiency of the coated grating is greater than 95% over a wide range of coating thicknesses. The maximum efficiency of 99.8% occurs at $\rho = 0.304$. This curve was calculated with a truncation order $N = 17$, and the error in the sum of efficiencies was smaller than 1.0×10^{-10} for all the points calculated.

The second example, shown in Fig. 4, is for an eight-layer-coated aluminum (Al, $n = 1.15 + i7.15$) grating. The coating materials are the same as those in Fig. 3, but here, adjacent to the Al substrate, is a Na_3AlF_6 layer. The bare Al grating has a peak efficiency of 88.7% at the chosen groove depth $h = 0.12\ \mu$m. Adding eight layers of coatings boosts the maximum efficiency to approximately 99.7% at $\rho = 0.304$. This curve was calculated with a truncation order $N = 19$.

In Fig. 5 the differences between unity and the first-order efficiencies of the two gratings considered in Figs. 3 and 4, with the coating thicknesses fixed at $\rho = 0.304$, are plotted against the number of coated layers. Clearly, these differences decrease exponentially as the number of layers increases. The vertical offset between these two sets of data roughly corresponds to the ratio between the efficiencies of the two gratings before the coatings are applied. From a practical point of view, one rarely needs to have more than 8 coated layers for the Al grating or more than 15 layers for the SiO_2 grating.

The angular dependencies of the efficiencies of the two gratings quoted in Figs. 3 and 4 are shown in Fig. 6. The coating thicknesses are fixed at $\rho = 0.304$. Note that the efficiencies of both gratings exceed 99% over an angular span of 12°. The fact that the two curves closely follow each other suggests that the angular behavior of a high-efficiency coated grating is predominantly determined by the grating profile and the coating materials rather than by the substrate material.

7. DISCUSSION

The diffraction efficiency curves in Figs. 3–6 exhibit a striking resemblance to the reflectivity curves of a multilayer thin-film reflector. Of course, the underlying physical principle for both types of device is that of optical interference, but the detailed light–medium interaction occurring in a multilayer-coated grating is much more complicated than that occurring in a multilayer thin-film reflector. The high-efficiency characteristics shown in these figures become even more amazing when one realizes that the curves are for a nonzero diffraction order and that nowhere along the grating contour do the incident light and the diffracted light locally obey the law of reflection. The basic principles and the design techniques for thin-film optical filters are fully developed and well documented.[20] For multilayer-coated gratings, however, much awaits to be developed.

Historically, high-efficiency reflection (surface-relief) gratings have been exclusively made of metallic materials. The examples of multilayer-coated gratings in Section 6 suggest that it is possible to make high-efficiency gratings with the use of dielectric materials only. The ratio of grating groove depth to period in this case is not at all demanding from a fabrication point of view. The wide and flat top of the high-efficiency peak makes control of the coating thickness forgiving. The thin-film deposition of many high-index and low-index materials is a mature and inexpensive process. Despite all these merits, needless to say, the theoretical predictions need to be verified experimentally. (In the paper of Mashev and Popov[13] a maximum diffraction efficiency of 70% was achieved with a nine-layer dielectric coated system.)

A fundamental limitation of the C method is its reliance on the assumption that the top surface contour of every coated layer perfectly replicates the initial grating profile. Such an assumption is not strictly valid in reality, however. The effects of imperfect replication on the diffraction anomalies of low-efficiency gratings have been studied by DeSandre and Elson.[5] For high-efficiency gratings the effects of imperfect replication on grating efficiency have yet to be investigated.

8. CONCLUSIONS

The differential method of Chandezon *et al.* for multilayer-coated gratings has been improved so that the computation time, especially for gratings in conical mountings, is greatly reduced and the previously existing limitations on the total coating thickness and on the total number of coatings are removed. The numerical examples have shown that a computer program that is based on the improved C method and equipped with the R-matrix propagation algorithm is capable of producing convergent results for gratings coated with several dozen dielectric layers of total coating thickness exceeding ten wavelengths without any numerical difficulty. This newly achieved computational ability has opened possible designs of multilayer-coated gratings that have not been attempted before.

APPENDIX A

In order to define succinctly the four Z matrices that are used in Section 3, I first define some auxiliary notation:

$$L_m(\eta) = \frac{1}{d}\int \exp[i\eta a(x) - imKx]\mathrm{d}x, \tag{A1}$$

where η is a dummy variable and the integration is over one grating period,

$$A_{mn}(\eta) = \alpha_m L_{m-n}(\eta), \tag{A2}$$

$$B_{mn}^{(\pm1)}(\eta) = \frac{\tilde{k}^{(\pm1)2} - \alpha_m\alpha_n}{\beta_n^{(\pm1)}} L_{m-n}(\eta), \tag{A3}$$

$$K_{1mq}^{(\pm1)} = \sum_{l=1}^{N} L_{m-l}[-\lambda_q^{(\pm1)}]W_{1lq}^{(\pm1)}, \tag{A4a}$$

$$K_{2mq}^{(\pm1)} = \sum_{l=1}^{N} L_{m-l}[-\lambda_q^{(\pm1)}]W_{2lq}^{(\pm1)}, \tag{A4b}$$

$$K_{3mq}^{(\pm1)} = \sum_{l=1}^{N} L_{m-l}[-\lambda_q^{(\pm1)}] \times [-\tau_1^{(\pm1)}\lambda_q^{(\pm1)}W_{1lq}^{(\pm1)} + \tau_3^{(\pm1)}\alpha_m W_{2lq}^{(\pm1)}], \tag{A4c}$$

$$K_{4mq}^{(\pm1)} = \sum_{l=1}^{N} L_{m-l}[-\lambda_q^{(\pm1)}] \times [+\tau_3^{(\pm1)}\alpha_m W_{1lq}^{(\pm1)} + \tau_2^{(\pm1)}\lambda_q^{(\pm1)}W_{2lq}^{(\pm1)}], \tag{A4d}$$

where the $W^{(\pm1)}$ are matrices formed by juxtaposition of the eigenvectors of matrix M for the two transition media

and the subscripts 1–4 for the matrices $K^{(\pm 1)}$ and $W^{(\pm 1)}$ designate the block rows of these matrices when they are written in a 4×1 block form. With this new notation the Z matrices are defined in the following block forms with the block sizes specified by the ranges of the indices:

$$Z_f^{(+1)} = \begin{bmatrix} L_{m-l}[\beta_l^{(+1)}] & 0 & W_{1mq}^{(+1)} & L_{m-n}[-\beta_n^{(+1)}] & 0 \\ 0 & L_{m-l}[\beta_l^{(+1)}] & W_{2mq}^{(+1)} & 0 & L_{m-n}[-\beta_n^{(+1)}] \\ -\tau_1^{(+1)} B_{ml}^{(+1)}[\beta_l^{(+1)}] & \tau_3^{(+1)} A_{ml}[\beta_l^{(+1)}] & W_{3mq}^{(+1)} & -\tau_1^{(+1)} B_{mn}^{(+1)}[-\beta_n^{(+1)}] & \tau_3^{(+1)} A_{mn}[-\beta_n^{(+1)}] \\ \tau_3^{(+1)} A_{ml}[\beta_l^{(+1)}] & \tau_2^{(+1)} B_{ml}^{(+1)}[\beta_l^{(+1)}] & W_{4mq}^{(+1)} & \tau_3^{(+1)} A_{mn}[-\beta_n^{(+1)}] & \tau_2^{(+1)} B_{mn}^{(+1)}[-\beta_n^{(+1)}] \end{bmatrix}, \quad \text{(A5a)}$$

with

$$l \in U^{(+1)}, \quad m \in U, \quad n \in U, \quad q \in V^{(+1)}; \quad \text{(A5b)}$$

$$Z_f^{(-1)} = \begin{bmatrix} L_{m-l}[\beta_l^{(-1)}] & 0 & L_{m-n}[-\beta_n^{(-1)}] & 0 & W_{1mq}^{(-1)} \\ 0 & L_{m-l}[\beta_l^{(-1)}] & 0 & L_{m-n}[-\beta_n^{(-1)}] & W_{2mq}^{(-1)} \\ -\tau_1^{(-1)} B_{ml}^{(-1)}[\beta_l^{(-1)}] & \tau_3^{(-1)} A_{ml}[\beta_l^{(-1)}] & -\tau_1^{(-1)} B_{mn}^{(-1)}[-\beta_n^{(-1)}] & \tau_3^{(-1)} A_{mn}[-\beta_n^{(-1)}] & W_{3mq}^{(-1)} \\ \tau_3^{(-1)} A_{ml}[\beta_l^{(-1)}] & \tau_2^{(-1)} B_{ml}^{(-1)}[\beta_l^{(-1)}] & \tau_3^{(-1)} A_{mn}[-\beta_n^{(-1)}] & \tau_2^{(-1)} B_{mn}^{(-1)}[-\beta_n^{(-1)}] & W_{4mq}^{(-1)} \end{bmatrix}, \quad \text{(A6a)}$$

with

$$l \in U, \quad m \in U, \quad n \in U^{(-1)}, \quad q \in V^{(-1)}; \quad \text{(A6b)}$$

$$Z_g^{(+1)} = \begin{bmatrix} \delta_{ml} & 0 & K_{1mq}^{(+1)} & \delta_{mn} & 0 \\ 0 & \delta_{ml} & K_{2mq}^{(+1)} & 0 & \delta_{mn} \\ -\tau_1^{(+1)} B_m^{(+1)} \delta_{ml} & \tau_3^{(+1)} \alpha_m \delta_{ml} & K_{3mq}^{(+1)} & \tau_1^{(+1)} \beta_m^{(+1)} \delta_{mn} & \tau_3^{(+1)} \alpha_m \delta_{mn} \\ \tau_3^{(+1)} \alpha_m \delta_{ml} & \tau_2^{(+1)} \beta_m^{(+1)} \delta_{ml} & K_{4mq}^{(+1)} & \tau_3^{(+1)} \alpha_m \delta_{mn} & -\tau_2^{(+1)} \beta_m^{(+1)} \delta_{mn} \end{bmatrix}, \quad \text{(A7a)}$$

with

$$l \in U^{(+1)}, \quad m \in U, \quad n \in U, \quad q \in V^{(+1)}; \quad \text{(A7b)}$$

and

$$Z_g^{(-1)} = \begin{bmatrix} \delta_{ml} & 0 & \delta_{mn} & 0 & K_{1mq}^{(-1)} \\ 0 & \delta_{ml} & 0 & \delta_{mn} & K_{2mq}^{(-1)} \\ -\tau_1^{(-1)} B_m^{(-1)} \delta_{ml} & \tau_3^{(-1)} \alpha_m \delta_{ml} & \tau_1^{(-1)} \beta_m^{(-1)} \delta_{mn} & \tau_3^{(-1)} \alpha_m \delta_{mn} & K_{3mq}^{(-1)} \\ \tau_3^{(-1)} \alpha_m \delta_{ml} & \tau_2^{(-1)} \beta_m^{(-1)} \delta_{ml} & \tau_3^{(-1)} \alpha_m \delta_{mn} & -\tau_2^{(-1)} \beta_m^{(-1)} \delta_{mn} & K_{4mq}^{(-1)} \end{bmatrix}, \quad \text{(A8a)}$$

with

$$l \in U, \quad m \in U, \quad n \in U^{(-1)}, \quad q \in V^{(-1)}. \quad \text{(A8b)}$$

It can be shown that, for sufficiently large N, $[V^{(+1)}] + 2[U^{(+1)}] = [V^{(-1)}] + 2[U^{(-1)}] = 2N$, where the square brackets denote the number of elements in the set being enclosed. Thus $Z_f^{(\pm 1)}$ and $Z_g^{(\pm 1)}$ are square matrices.

APPENDIX B

The C method requires the evaluation of three Fourier expansion coefficients, C_m, D_m, and L_m, which are defined, respectively, in Eqs. (7), (8), and (A1). For a sinusoidal grating profile

$$a(x) = \frac{h}{2}[1 - \cos(Kx)] \quad \text{(B1)}$$

these coefficients have simple analytical expressions:

$$C_m = \begin{cases} 0 & m \text{ odd} \\ \dfrac{1}{(1+p^2)^{1/2}} \left[\dfrac{p}{1+(1+p^2)^{1/2}} \right]^{|m|} & m \text{ even} \end{cases}, \quad \text{(B2)}$$

$$D_m = \begin{cases} 0 & m \text{ even} \\ \operatorname{sgn}(m) \dfrac{-i}{(1+p^2)^{1/2}} \left[\dfrac{p}{1+(1+p^2)^{1/2}} \right]^{|m|} & m \text{ odd} \end{cases}, \quad \text{(B3)}$$

where $p = \pi h/d$, and

$$L_m(\eta) = i^m \exp\left(i\frac{h}{2}\eta\right) J_m\left(-\frac{h}{2}\eta\right), \tag{B4}$$

where J is the Bessel function. Note that the coefficients C_m and D_m converge to zero geometrically.

REFERENCES

1. L. Li, "Multilayer modal method for diffraction gratings of arbitrary profile, depth, and permittivity," J. Opt. Soc. Am. A **10,** 2581–2591 (1993).
2. M. G. Moharam and T. K. Gaylord, "Diffraction analysis of dielectric surface-relief gratings," J. Opt. Soc. Am. **72,** 1385–1392 (1982).
3. D. Maystre, " A new general integral theory for dielectric coated gratings," J. Opt. Soc. Am. **68,** 490–495 (1978).
4. D. Maystre, "A new theory for multiprofile, buried gratings," Opt. Commun. **26,** 127–132 (1978).
5. L. F. DeSandre and J. M. Elson, "Extinction-theorem analysis of diffraction anomalies in overcoated gratings," J. Opt. Soc. Am. A **8,** 763–777 (1991).
6. J. Chandezon, M. T. Dupuis, G. Cornet, and D. Maystre, "Multicoated gratings: a differential formalism applicable in the entire optical region," J. Opt. Soc. Am. **72,** 839–846 (1982).
7. D. Maystre, "Rigorous vector theories of diffraction gratings," in *Progress in Optics*, E. Wolf, ed. (Elsevier, Amsterdam, 1984), Vol. 21, pp. 1–67.
8. J. Chandezon, D. Maystre, and G. Raoult, "A new theoretical method for diffraction gratings and its numerical application," J. Opt. (Paris) **11,** 235–241 (1980).
9. E. Popov and L. Mashev, "Conical diffraction mounting generalization of a rigorous differential method," J. Opt. (Paris) **17,** 175–180 (1986).
10. S. J. Elston, G. P. Bryan-Brown, and J. R. Sambles, "Polarization conversion from diffraction gratings," Phys. Rev. B **44,** 6393–6400 (1991).
11. E. Popov and L. Mashev, "Convergence of Rayleigh–Fourier method and rigorous differential method for relief diffraction gratings," Opt. Acta **33,** 593–605 (1986).
12. E. Popov and L. Mashev, "Convergence of Rayleigh–Fourier method and rigorous differential method for relief diffraction gratings—non-sinusoidal profile," Opt. Acta **34,** 155–158 (1987).
13. L. Mashev and E. Popov, "Diffraction efficiency anomalies of multicoated dielectric gratings," Opt. Commun. **51,** 131–136 (1984).
14. E. J. Post, *Formal Structure of Electromagnetics* (North-Holland, Amsterdam, 1962), Chap. 3, p. 47.
15. E. Popov and L. Mashev, "Rigorous electromagnetic treatment of planar corrugated waveguides," J. Opt. Commun. **7,** 127–131 (1986).
16. J. Chandezon, "Les équations de Maxwell sous forme covariante, application a l'étude de la propagation dans les guides périodiques et a la diffraction par les réseaux," Ph.D. dissertation (University of Clermont-Ferrand II, France, 1979).
17. See, for example, R. A. Horn and C. R. Johnson, *Matrix Analysis* (Cambridge U. Press, Cambridge, U.K., 1985), Chap. 1, Section 4, pp. 59–64.
18. S. L. Chuang and J. A. Kong, "Wave scattering from a periodic dielectric surface for a general angle of incidence," Radio Sci. **17,** 545–557 (1982).
19. D. Maystre, J. P. Laude, P. Gacoin, D. Lepere, and J. P. Priou, "Gratings for tunable lasers: using multidielectric coatings to improve their efficiency," Appl. Opt. **19,** 3099–3102 (1980).
20. See, for example, H. A. Macleod, *Thin Film Optical Filters*, 2nd ed. (Adam Hilger, Bristol, U.K., 1986).